Scientific paper

Three-dimensional Nonlinear Bond Model incorporating Transverse Action in Corroded RC Members

Feng Shang[1], Xuehui An[2], Tetsuya Mishima[3] and Koichi Maekawa[4]

Received 22 August 2010, accepted 21 January 2011

Abstract

Reinforcing bar corrosion induces splitting cracks in concrete along the bar axis and leads to bond deterioration. This can adversely affect the crack spacing in an RC member and have a serious effect on its serviceability. This study looks at axial nonlinearity in corroded RC members under tension and shows that fewer transverse cracks with greater spacing occur as steel corrosion progresses. The open-slip coupled model, which takes into account the transverse action associated with longitudinal bond stress transfer in the bond transition zone, is extended to cover corroded reinforcement and is successfully used to simulate the behavior of RC members in tension. Modeling of the bond transition zone and of the layer of corrosion products is found to be crucial to understanding residual bond performance after corrosion has occurred.

1. Introduction

Reinforced concrete (RC) members exposed to chloride attack are vulnerable to corrosion. In general, chloride ions migrate into the concrete through the surface and cause depassivation of protective oxide layers on the surfaces of reinforcing bars, which in the end leads to corrosion. Corrosion products fill the concrete-steel interface and volume expansion initiates splitting of the concrete cover. As a result, the bond between steel and concrete may deteriorate significantly (Al-Sulaimani *et al*. 1990; Amleh *et al*. 1999; Auyeung *et al*. 2000; Fang *et al.* 2004).

Besides the question of the remaining reinforcement capacity of these corroded members (Rodriguez *et al*. 1997; Coronelli and Gambarova 2004), their residual serviceability may raise a critical engineering issue with regard to life cycle assessment and management (Enright *et al.* 1998; Li 2003). Among the factors affecting serviceability, including crack width and deflection, residual bonding plays an important role (Zhang, *et al.* 2009) and the magnitude of its deterioration needs to be quantitatively evaluated.

The one dimensional (1D) bond-slip models have been developed for evaluation of crack width and seismic assessment in engineering practice (Hawk *et al.* 1982; Chou *et al.* 1983; Shima *et al.* 1987; Červenka, 2002). These models are so powerful solely for axial nonlinearity simulation of RC members free from corrosion in tension. But, the 1D models may no longer treat the transverse action that causes splitting cracks of concrete cover along reinforcing bars (Tepfers 1979; Xu *et al*. 1994; Fardis 2009). It must be noted that the splitting cracks are more frequently found in corroded RC members because of the coupling effect of ring tension and corrosion pressure around bars. Then, the model of corroded RC members should have a capability to treat the mechanistic ring tension stress field concurrently.

In the past decade, lots of effort (Coronelli 2002; Berra *et al.* 2003; Lundgren 2005, 2007; Amleh *et al.* 2006) has been made to investigate residual bonding action after corrosion. The focus has been on the corrosion-induced pressure at the concrete-bar interface and this has been found to be greatly affected by the state of confinement; e.g., the presence of web reinforcement and/or a skin steel. Different approaches to the study of corrosion pressure have been reported in the literature. Berra *et al*. (2003) model the rib geometry by finite element analysis in which an inherent corrosion pressure is assumed, while Lundgren (2005, 2007) and Amleh (2006) use friction models for the relationship between bond stress and interfacial pressure.

However, the effect of reinforcing bar strain on local bonding characteristics has rarely been incorporated into numerical models. Consequently, these models are implicitly forced into an unrealistic assumption; i.e., they assume that the local bond-slip relation is rigidly defined in structural analysis regardless of the location of, or damage to, the bond transition zone.

As a matter of fact, detailed experimental observations by Chou *et al*. (1983) have proved that the local bond-slip relation in axial tension as well as the results of pull-out tests using bars with relatively short embedded length depend on the location. This location-dependent relation between bond stress and slip

[1]Research Associate, State Key Laboratory of Hydro Science and Engineering, Tsinghua University, P. R. China.
E-mail: shangf00@mails.thu.edu.cn
[2]Professor, State Key Laboratory of Hydro Science and Engineering, Tsinghua University, P. R. China.
[3]Managing Engineer, Maeda Corporation, Japan.
[4]Professor, Department of Civil Engineering, The University of Tokyo, Japan.

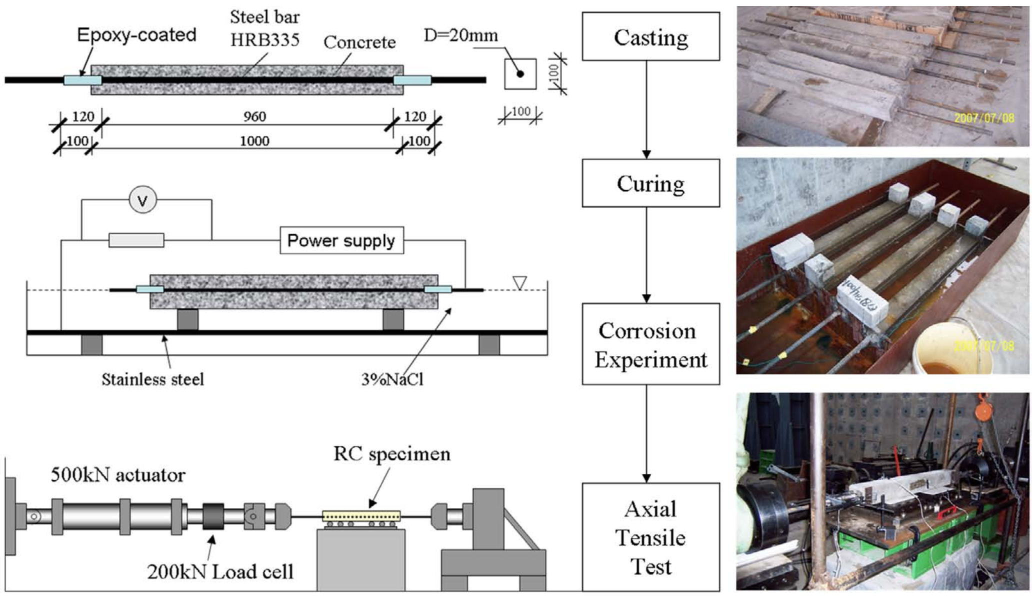

Fig. 1 Experiment details.

was successfully generalized into the concept of strain-dependent local bond stress-slip by Chou *et al.* (1983). The local bond stress is reduced where the longitudinal reinforcement strain increases, a behavior that is thought to denote micro defects in a bond transition zone with bond cracks (Goto 1971; Maekawa *et al.* 2003).

Shima *et al.* (1987) implemented pull-out experiments with a long embedded steel bar and an aluminum bar with the same geometry, respectively, and showed that the local bond stress of the aluminum bar is smaller than that of the steel owing to the greater strain in the aluminum bar at a particular location. This provides further direct proof of the strain effect.

The authors of this work fully accept this understanding as a fundamental core part of the bond mechanism and adopt it in the newly developed open-slip coupled model (Shang *et al.* 2010), which is capable of simulating both three-dimensional confinement, the ring-tension stress field, and the effects of bar strain on bonding within a finite element analysis scheme. Here, the term 'strain effect' will be used as shorthand for this effect.

The objective of this study is to extend the three-dimensional open-slip coupled model to include the case of corroded reinforcement, clarifying the effect of transverse action and damage in the bond transition zone and that of steel corrosion on the remaining bond with regard to crack spacing in corroded RC members. To verify the analytical model, axial tensile loading experiments are carried out on corroded RC members set up systematically with various parameters.

2. Crack spacing of corroded RC members in tension

In this section, the authors discuss the uniaxial tension loading experiment carried out using corroded RC members. **Figure 1** shows that all specimens have the same cross section (100mm*100mm) and the same length (1000mm), each also having a 20mm reinforcing bar embedded at the center of the cross-section. The relatively large reinforcement ratio (3.14%) and large relative length are selected so as to ensure large numbers of transverse cracks even after corrosion cracking of different magnitudes; this means that reliable macroscopic nonlinear events are obtained reliably. A total of 10 specimens are studied.

Following curing for 28 days after casting, galvanostatic-corrosion was imposed on each specimen using a constant current power supply to control the corrosion crack width. A 20mm length of the edged steel bar at each end of each specimen is coated with epoxy resin before casting to avoid localized corrosion.

After each specimen received a certain amount of electric charge, the galvanostatic corrosion was terminated and the corrosion-induced crack width was recorded. Thereafter, a static tensile force was applied to each damaged specimen; the corroded RC specimen was laid horizontally and supported on rollers and plastic plates to reduce friction with the supports on the floor. Clear splitting crack was found on specimen-A11 followed by spalling of concrete cover even though the specimen was loosely wrapped with cloth during loading tests as protection. Then, the concrete pieces were securely sustained after the spalling.

Any transverse cracking was carefully monitored during the loading experiments and marked on the surface of each specimen. Loading continued until no more transverse cracks appeared. After loading, the cover concrete was removed and the weight loss of the corroded bar was measured.

Table 1 summarizes the concrete compressive strength at loading time, the degree of corrosion, the maximum number of transverse cracks, the applied load at initiation of the first transverse crack, and the ultimate capacity. A few shrinkage cracks (less than 0.1mm wide) were observed close to the edge of some specimens before the loading test.

Even though concrete shrinkage may affect transverse crack spacing, comparatively small numbers of transverse cracks were observed in the corroded cases. Furthermore, the greater the splitting crack width caused by corrosion-induced ring tension, the smaller the number of transverse cracks produced (that is, the average transverse crack spacing increases). The cloth-wrapped Specimen-A11 exhibits more transverse cracks than Specimen-A10, despite the high corrosion loss of the latter. This is thought to be attributable to the three-dimensional confinement effect on the bond.

Similar experimental results have been reported by Amleh *et al*. (2006), as shown in **Table 2**. Most correspond to cases of severe corrosion (greater than 10% of the corrosion loss) and wide splitting cracks (greater than 3mm). Hence, most of the experimental cases lined up in **Table 1** fall within the middle or light corrosion range, which is more often encountered in practice.

This behavior can be explained by microscopic deformation in the concrete-steel transition zone caused by corrosion of the reinforcement, resulting in less local bond stress. Thus, a greater development length along the bar is needed for transverse cracking to occur in the specimen. The ultimate number of cracks that develops may represent the magnitude of corrosion and the reduced stiffness of the RC member in tension. With this understanding, cases A1 to A10 are thought to be appropriate for use in verifying the simulation developed in this work. The experimentally obtained relations for load-elongation for each specimen are shown along with the crack patterns in the appendix.

3. Modeling of transverse action – open-slip coupled model

When the bond action arises together with the rust production to case corrosion pressure, the ring or hoop ten-

Table 1 Results of post-corrosion axial tensile experiment.

Specimen	Concrete strength at loading time f_c' (MPa)	Corrosion loss	Average splitting crack width (mm)	Load at the appearance of first transverse crack (KN)	Ultimate load applied in the test (KN)	Number of transverse cracks
A1	43.4	0.0%	0.00	23.5	125.0	8
A2	41.4	0.0%	0.00	24.0	125.0	8
A3	45.1	0.6%	0.00	Before load	125.0	9
A4	49.6	1.6%	0.20	Before load	125.0	7
A5	34.4	2.2%	0.10	20.0	125.0	7
A6	48.1	2.0%	0.40	Before load	125.0	7
A7	37.4	2.5%	0.55	10.0	90.0	6
A8	42.0	3.9%	1.78	14.0	90.0	4
A9	42.7	5.7%	1.45	10.0	90.0	5
A10	43.5	7.4%	3.80	6.0	90.0	1
A11	45.1	8.1%	Cover spalling	10.0	90.0	2

Table 2 Axial tensile experiment on corroded RC specimens by Amleh *et al*. (2006).

Specimen	Corrosion loss	Measured splitting crack width (mm)	Load at the appearance of first transverse crack (KN)	Ultimate load applied in the test (KN)	Number of transverse cracks
SS1	0.0%	0.00	12.0	127.0	10
SS2	0.0%	0.00	12.5	127.0	10
CS1	4.0%	0.15	15.0	125.0	9
CS2	5.5%	0.20	2.3	124.0	8
CS3	11.0%	6.0	2.93	115.0	3
CS4	11.5%	1.5~3.0	1.27	112.0	5
CS5	12.0%	1.5~4.0	0.64	111.0	3
CS6	17.5%	9.0	-	100.0	0

sion around the bar will be magnified. Then, for the mechanistic analysis of bond of corroded reinforcing bar, ring-tension must be consistently presented in the numerical simulation approach. To meet the challenge, the authors select the open-slip coupled model of bond (Shang *et al*. 2010) as the simulation platform.

As illustrated in **Fig. 2**, the bond transition zone is defined as a cylindrical finite volume of concrete that encompasses the induced periodic local cracks associated with the lugs of the deformed reinforcing bar (Goto 1971). The thickness of this bond transition zone is of the same order as the bar radius. Both longitudinal and transverse forces are transferred through this transition zone to the large outer volume of concrete solids. The open-slip coupled model (Shang *et al*. 2010) is a simple representation of the 3D kinematics of this bond transition zone, which is a zone of locally high complexity. The direction of transferred stress is not parallel to the longitudinal axis of the bar; rather, there is also a transverse component of stress. In three-dimensional analysis, a rational formulation of this component is crucial so as to ensure that so-called ring (or hoop) tension as well as cracking along the bar arises. The open-slip model represents the stress field of bond transition zone by assuming an imaginary tilted slope. Deformational kinematics is represented by the relative displacement of the two tubular surfaces of the transition zone between which the micro-bond cracking (Goto crack) takes place. The extension and opening of bond cracks are converted into equivalent relative displacements in the longitudinal and transverse directions. If concrete is assumed to be a rigid body, the displacement kinematics is simply converted to the open-slip micro-plane as also illustrated in **Fig. 2**. Here, the plane is set skewed according to the bond crack direction (Goto 1971). Then, the imaginary shear slip along the micro-plane mostly corresponds to the width of the local bond cracks, and the kinematics normal to the micro-plane is thought to be associated with inelasticity in compression.

Open-slip at the micro level (u_n, v_n) on the micro-plane is linked with the macro-level open-slip (ω and δ) along the bond transition zone as,

$$\begin{cases} u_n = \delta \sin\theta - \omega\cos\theta \\ v_n = \delta\cos\theta + \omega\sin\theta \end{cases} \tag{1}$$

where θ is the inclined angle of the micro-plane.

Here, the bond stress denoted by τ and the dilatant stress p on the bond transition zone may be derived from the micro-plane stresses σ_n and τ_n by coordinate transformation as,

$$\begin{aligned} \tau &= \frac{1}{L}\left(\sigma_n \sin\theta + \tau_n\cos\theta\right) \\ p &= \frac{1}{L}\left(-\sigma_n\cos\theta + \tau_n\sin\theta\right) \end{aligned}, \quad \tau_\varphi = E_\varphi\delta_\varphi \tag{2}$$

where L denotes the spacing of bar lugs; and τ_φ, E_φ, and δ_φ are the torsional shear stress, average stiffness, and twist angle around the axis of the bar. As a matter of fact, the torsional degree of freedom is unavoidable in formulation where the mathematical completeness of 3D space is required. But, since torsion around the bar axis is minimal in general, linear elasticity with relatively large stiffness is assumed as above.

As reported by Shima *et al*. (1987), the local bond characteristics, which may develop over the bond tran-

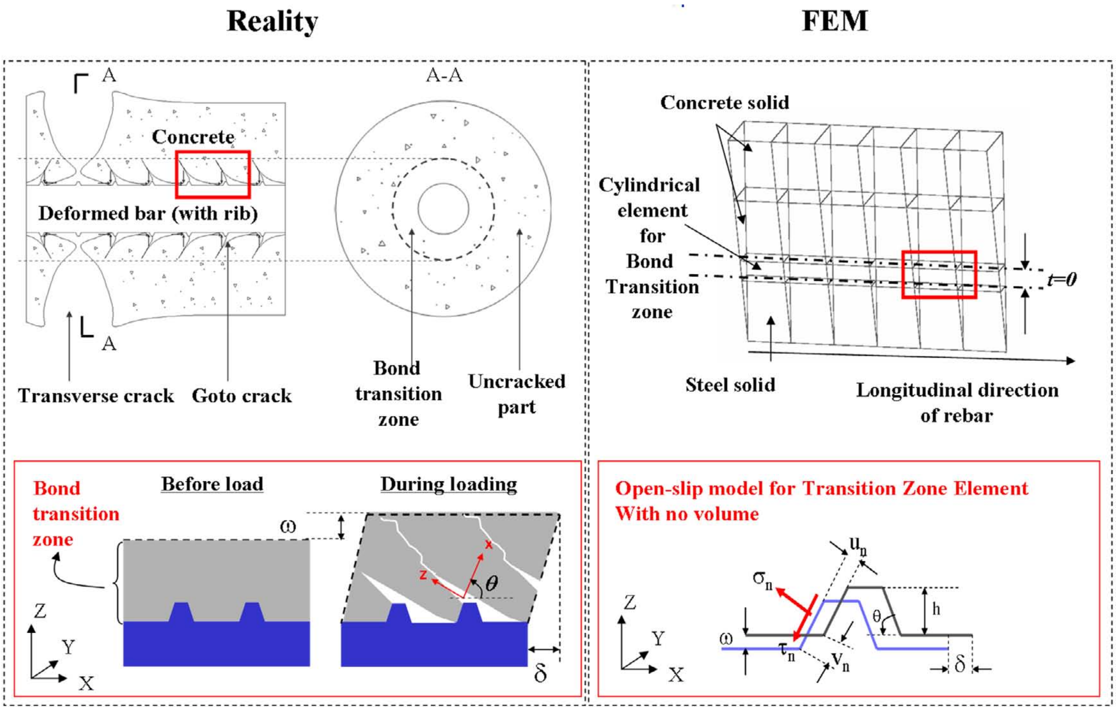

Fig. 2 Modeling of bond transition zone for finite element analysis.

sition zone, are strongly dependent on bar strain. The authors assume the same sensitivity in terms of bar strain as that proposed in Shima's original model (1987) as,

$$\sigma_{\mathrm{n}} = \frac{\sigma_{\mathrm{n}}^{0}}{1+\varepsilon\times 10^{\lambda}} \tag{3}$$

where σ_{n}^{0} denotes the intrinsic normal stress corresponding to ε=0 (see Equation (4)), and λ=3.5 (Shang *et al*. 2010). The bar strain is the averaged value for the bond transition zone of the concrete including bond cracking (Goto 1971), because concrete and steel share the same displacement at each bar lug.

In **Fig. 3**, which plots Eq. (3), it is clear that there is a large reduction in local contact stress when the longitudinal steel strain exceeds 100μ, which is approximately equal to the cracking strain of the concrete. For simplicity, the authors assume an elastic and perfectly plastic model, as follows:

$$\sigma_{\mathrm{n}}^{0} = f(u_n) = \begin{cases} \alpha E_{\mathrm{b}}^{0}(u_n - u_p), & u_n \geq u_p \\ 0, & u_n < u_p \end{cases} \tag{4}$$

where E_{b}^{0} is the equivalent stiffness of the inclined compression strut and α is its effective area. Taking an extreme condition, α will be nil when the macro-open mode of the bond transition zone exceeds the height of the bar ribs. Then, for simplicity, we have,

$$\alpha = \begin{cases} 1, & \omega < 0 \\ 1-\omega/h, & 0 \leq \omega \leq h \\ 0, & \omega > h \end{cases} \tag{5}$$

where h denotes the height of the rib.

The variable u_{p} indicates the plastic component of relative normal displacement, which is formulated as,

$$u_p = \begin{cases} u_{\max} - u_{\lim}, & u_{\max} \geq u_{\lim} \\ 0, & u_{\max} < u_{\lim} \end{cases} \tag{6}$$

where $u_{\max}$ is the maximum normal displacement in the loading history and $u_{\lim}$ is its elastic limit. Then, the local compression yielding strength, f_y, is calculated when the bond transition zone is completely closed as,

$$f_y = E_{\mathrm{b}}^{0} u_{\lim} \tag{7}$$

Li and Maekawa (1987) introduced the analogy of idealized inclined micro-plane interactions and contact density modeling for cracking shear transfer. Since the stiffness and strength of steel are much greater than those of concrete, contact stiffness E_{b}^{0} and local yield strength f_{y} can be defined in a similar manner to this cracking shear transfer (Maekawa *et al*. 2003) as,

$$\begin{cases} E_{\mathrm{b}}^{0} = 343 f_{\mathrm{c}}'^{(1/3)} \ \text{(MPa/mm)} \\ f_{\mathrm{y}} = 13.7 f_{\mathrm{c}}'^{(1/3)} \ \text{(MPa/mm)} \end{cases} \tag{8}$$

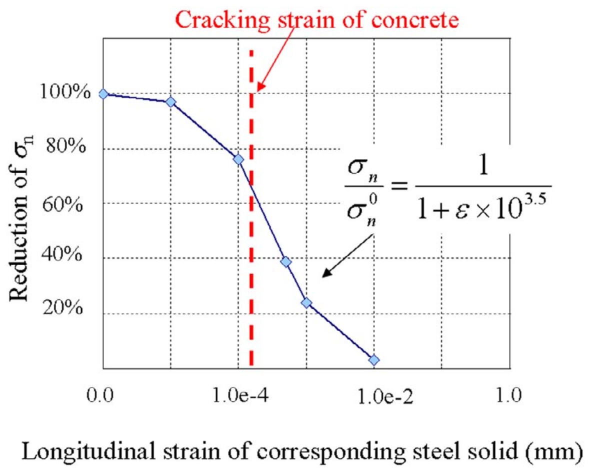

Fig. 3 Strain effect on local normal contact performance.

This is also analogous to local transverse action (friction) along the micro-plane. Then, we apply the Mohr-Coulomb law as,

$$\begin{cases} d\tau_n = \alpha G_n dv_n \\ \int_{path} d\tau_n \leq \mu\sigma_n \end{cases} \tag{9}$$

where G_{n} is the tangential stiffness along the micro-plane and v_{n} is the relative shear displacement. Then we have,

$$G_n = 0.5 E_b \tag{10}$$

According to experiments by Xu *et al*. (1994), μ is around 0.2-0.3 (in this paper, μ=0.25). By simultaneously solving equations (1)-(10), the three dimensional stress field developing inside the bond transition zone can be formulated. This modeling procedure as shown in **Fig. 4** has been verified for wide ranges of embedded length of reinforcement and concrete cover with and without splitting cracks (Shang *et al*. 2010). The authors

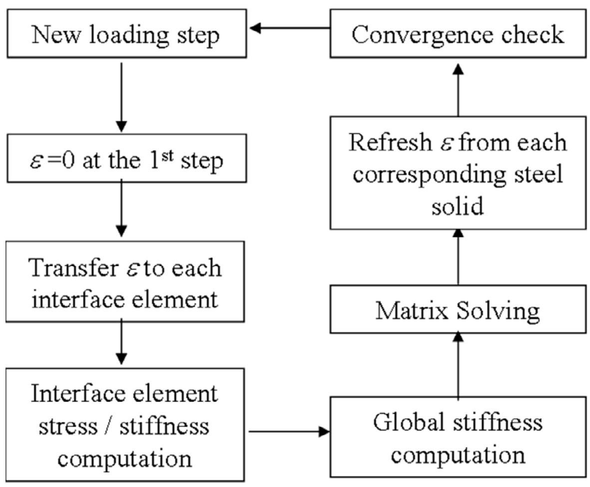

Fig. 4 Methodology for steel strain transfer in computation.

apply this open-slip coupled modeling method to corroded reinforcement in the following section.

4. Coupling model with corrosion products around steel bar

When corrosion products form around the steel bar, the bond transition zone exhibits mechanistic anisotropy (Toongoenthong *et al*. 2005) and this plays an important role in post-corrosion bond stress transfer (Lundgren 2005).

The corrosion coupled system in the longitudinal direction is assumed to consist of parallel springs, as shown in **Fig. 5**, one representing the bar with a reduced cross section and the other the rust layer. The axial stiffness of the corrosion products is negligible, so only the bar component is considered in the analysis. Here, the reduced modulus and yield strength of the steel solid is assumed proportional to the degree of corrosion.

As the depth of corrosion product layer is rather small (0-10^3μm) compared with the reinforcing bar diameter, the influence of this layer on the transverse action of the bond transition zone is formulated by extending the mechanical model in the radial direction based on the open-slip model. As corrosion products develop at the concrete-bar interface, a fictitious spring component can be used to represent it numerically. Then, the overall equivalent contact spring (see **Fig. 5**) can be written as,

$$\frac{1}{E_{\mathrm{b}}} = \frac{1}{E_{\mathrm{b}}^{0}} + \frac{1}{K_{\mathrm{cor}}} \tag{11}$$

$$K_{\mathrm{cor}} = \frac{d\sigma_{\mathrm{n}}}{d\eta} = \frac{G_{\mathrm{cor}}d\varepsilon}{d\eta} = \frac{G_{\mathrm{cor}}}{\eta} \tag{12}$$

where K_{cor} is the rigidity of the corrosive rust layer (MPa/mm), E_{b} is the equivalent stiffness at the interface after corrosion, E_{b}^{0} is the equivalent of E_{b}, as used in equations (3)-(12), for use in the computation of corroded cases, η is the thickness of corrosion products layer, and G_{cor} denotes the Young's modulus of the corrosion products (MPa).

A wide range of the Young's modulus values has been reported for steel corrosion products, including 0.02GPa (Yoshioka and Yonezawa 2002), 2-4GPa (Molina *et al.* 1993), 7GPa (Toongoenthong *et al*. 2005), and 14GPa (Lundgren 2002). In fact, the corrosion layer behaves like a granular material, with stiffness depending strongly on pressure (Lundgren 2002). Ouglova *et al.* (2006) claimed that the stress state of the corrosion products layer in reinforced concrete can be treated as similar to that of the assembled corrosion products in an oedometer test. **Figure 6** shows a typical stress-strain relation measured in oedometer tests by Ouglova *et al.* (2006). In this work, the relation is simplified into two linear stages denoting the confinement effect, with the lower confinement value of G_{cor} being around 100MPa.

Note that high interfacial pressure usually builds up before the occurrence of a splitting crack in the greater concrete cover (Lundgren. 2002) and in cases strongly confined by web reinforcement or skin reinforcement (Coronelli. 2002). However, for the experiment discussed in section 2 above, wide splitting cracks were observed in most of the corroded specimens and no web reinforcement was used. Hence, a small value of G_{cor} is expected. Here, G_{cor} is assumed to be 100MPa and the

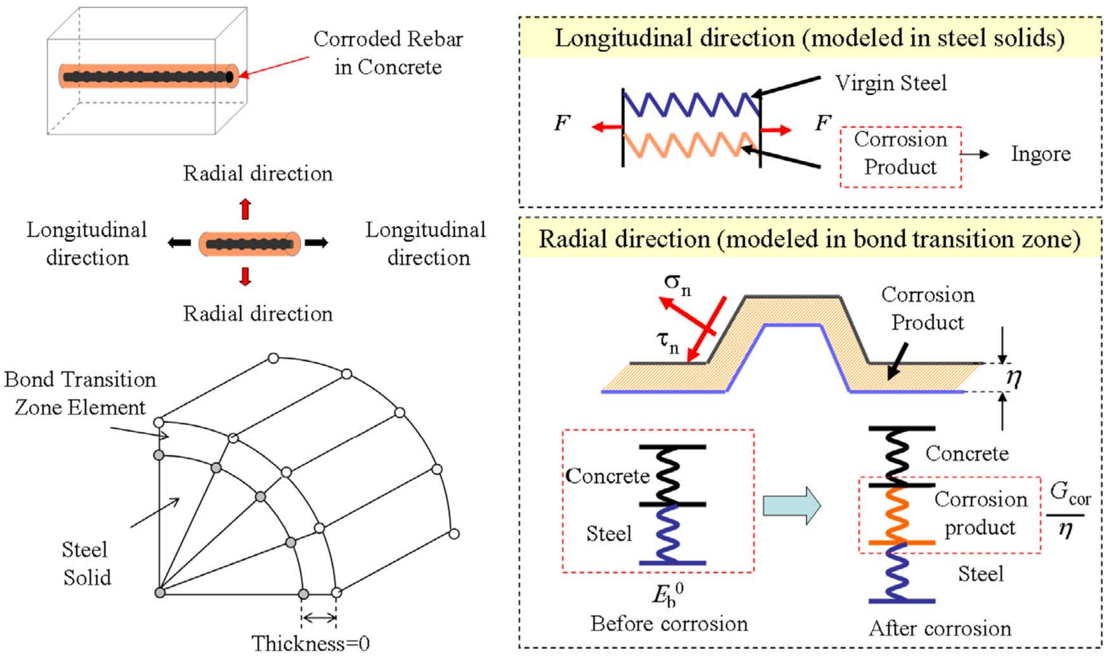

Fig. 5 Modeling of corrosion product impact inside the bond transition zone.

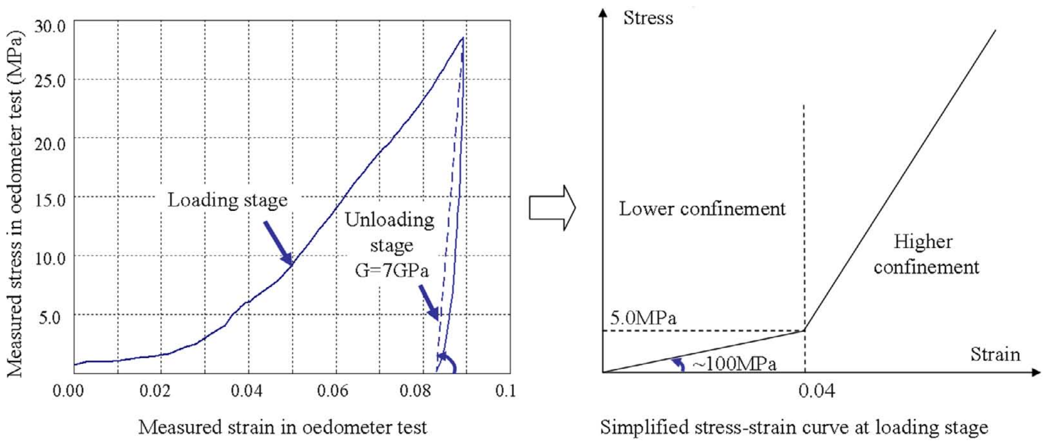

Fig. 6 Oedometer test result by Ouglova *et al*. (2006) and a simplification (compression as positive).

value is further checked in the sensitivity analysis.

5. Simulation of crack spacing in corroded RC

5.1 Analytical approach

The simulation of residual bonding after corrosion focuses on a pre-corroded specimen. First, splitting of the concrete cover resulting from expansion of the corrosion products is modeled by imposing an isotropic volumetric strain on the solid elements of the reinforcement. This action induces radial deformation without any elongation of the reinforcement. The resultant tensile stress arises in the concrete in the hoop direction, leading to splitting cracks in concrete solid elements, as shown in **Fig. 7**. Mesh-size dependency was checked in terms of convergence of nonlinear solution beforehand, and the allowable large sized elements similar to the mean size of coarse aggregates are arranged.

The bond transition zone is of much smaller extent than the concrete and the reinforcing bars, so the cylindrical thickness of this layer is ignored in the interface elements. The numerically induced volumetric expansion is terminated when the splitting crack reaches the same value as that observed in the experiment. After termination, analysis of loading is carried out.

The residual stress and strain states of the concrete solid and interface elements, as determined in the above first stage of analysis, are used as the initial values in the subsequent loading simulation. The residual states of the steel solid, on the other hand, are initialized. The effect of damaged concrete cover and confinement on bonding is consistently taken into account in the simulation. This stage of analysis is referred to as the 're-start' stage.

Figure 8 shows the finite element mesh used in this second stage of analysis. Three-dimensional (3D) quadrilateral isoparametric solid elements are used for both the reinforcing bars and the surrounding concrete. Zero-volume interface elements are placed between the reinforcement and the concrete, with behavior governed by the opening-slip coupled model for the bond transition zone. A one-eighth model with a symmetrical boundary is used. The reinforcement is assumed to be perfectly elastic. The surrounding concrete is modeled using the 3D multi-directional smeared crack approach so that the interaction between corrosion cracks and local bond cracks can be simulated. Details of the model are skipped here, but can be found in past research by Maekawa *et al.* (2003) in which the model is verified. Here, cracking of concrete is introduced normal to the direction of the maximum principal stress when the principal stresses exceed cracking criterion. The tension softening model of concrete is formulated after cracking in consideration of tensile fracture energy (Maekawa *et al*. 2003).

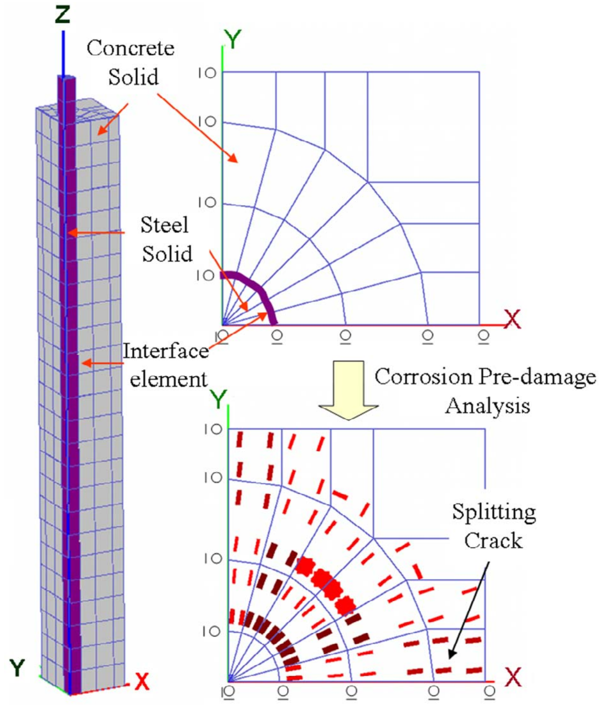

Fig. 7 FEM mesh for simulation of corrosion pre-damage analytical approach.

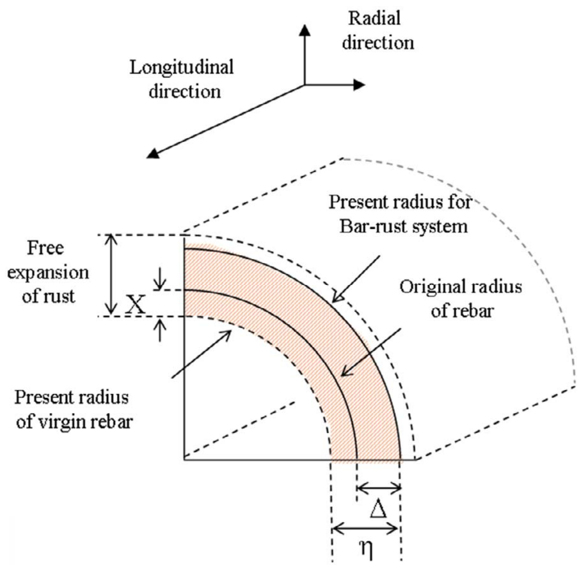

Fig. 8 FEM mesh for simulation and corrosion pre-damage analytical approach.

In order to take into account the effect of concrete shrinkage in a simplified manner, an apparently reduced tensile strength is used as,

$$f_t = \zeta(0.23 f_c'^{2/3}) \tag{13}$$

where ζ is a reduction coefficient taking into account the effect of self-equilibrated stress induced by concrete shrinkage. This is an empirical estimate of strength based on the JSCE code. In cases where shrinkage cracks are observed before loading, ζ is set to 0.5 while in other cases ζ is set to 0.7 according to past validations.

As shown in **Fig. 8**, the thickness η of the corrosion product layer is calculated as,

$$\eta = X + \Delta \tag{14}$$

where Δ is the difference between the present radius of the bar-rust system and the original radius of the virgin bar. Strictly speaking, Δ should be different from the value assuming a free expansion of the corrosion products, however it can be approximately calculated as follows:

$$\Delta = \varepsilon_{expan} D / 2 \tag{15}$$

where ε_{expan} is the input isotropic strain in the corrosion pre-damage analysis.

X is the equivalent penetration of corrosion products into the virgin steel and can be calculated as,

$$X = (1 - \sqrt{1 - \Omega}) D / 2 \tag{16}$$

where Ω is the corrosion loss obtained from the experiment results.

In this second 're-start' stage of analysis, η is automatically obtained from the results of the corrosion pre-damage analysis (the first stage), in which η is updated in each step to represent the growth of corrosion products. Here, Δ computed from the previous step is used to calculate η in the current step during the first stage of analysis.

Table 3 shows the input parameters used for the finite element simulation of each specimen.

5.2 Transverse action and damage in the bond transition zone after corrosion

Residual transverse action and deformation arise in the bond transition zone due to expansion of the corrosion products, whereas no longitudinal deformation or bond stress results from the corrosion process. Since the cylindrical thickness of the bond transition zone can be computationally ignored in interface elements, the terms 'open' and 'slip' are used to describe transverse and longitudinal deformation of the bond transition zone. 'Pressure' is the term used to describe the transverse force. **Figure 9** shows the computed results for the corrosion pre-damage stage in the case of specimen A10. The states of other specimens are also indicated in the

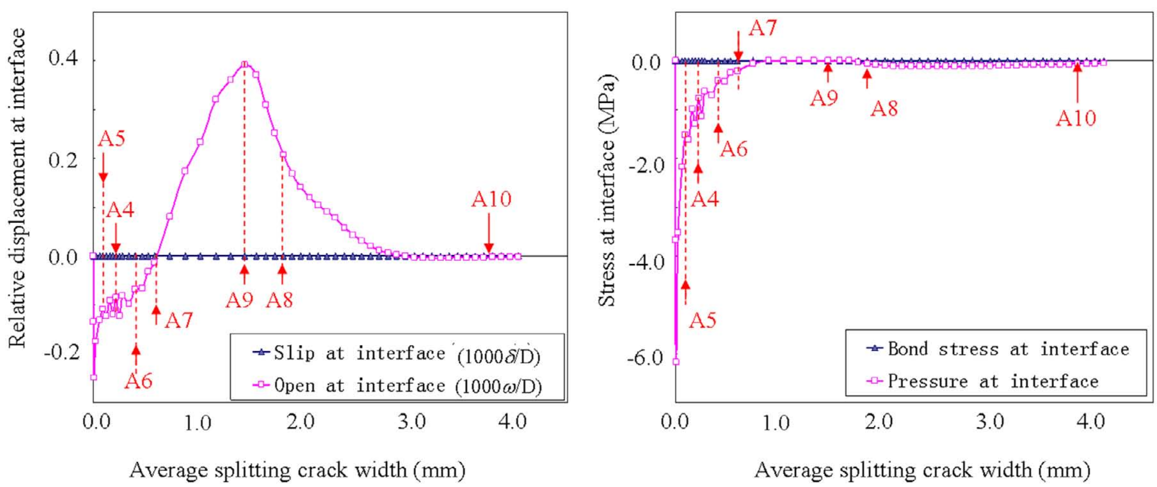

Fig. 9 Computed results of interface element in corrosion pre-damage analysis.

Table 3 Input parameters for simulation of each specimen in section 2.

Specimen	Steel solid	Concrete solid	Interface element		
	ε_{expan}	f_t (MPa)	E_b^0(MPa/mm)	f_y (MPa)	η (μm)
A1	0.0	2.0	1205.38	48.14	0.0
A2	0.0	2.0	1186.57	47.39	0.0
A3	0.003	1.5	1220.92	48.77	60.0
A4	0.008	1.5	1260.24	50.34	160.0
A5	0.005	1.7	1115.53	44.56	161.0
A6	0.016	1.5	1247.41	49.82	261.0
A7	0.018	1.8	1147.06	45.82	308.0
A8	0.070	1.9	1192.28	47.62	895.0
A9	0.050	1.9	1198.86	47.88	789.0
A10	0.160	1.9	1206.31	48.18	1979.0

figure. It is clear that pressure builds up in the bond transition zone prior to the occurrence of a splitting crack, while pressure falls dramatically as the splitting crack increases in width.

It is noteworthy that the transverse deformation switches from closure to opening when the splitting crack exceeds 0.5mm in width, where transverse deformation is the total compressive/tensile deformation of the corroded layer and the local concrete in front of the rib. This hints at possible damage in the bond transition zone after corrosion. Consequently, greatly reduced bond performance might be expected in the second stage of analysis. If seen, this would effectively illustrate the effect of confinement on bonding.

Also worth noting is the decreasing relative displacement as the splitting crack grows wider and wider; almost no pressure is developed during this time. This represents a complete loss of confinement by the concrete and free expansion of the corrosive product.

5.3 Simulation of residual bond performance in corroded RC members

As already noted, the second 're-start' stage of analysis adopts the residual stress-strain information obtained in the section above as the initial conditions. The computed 1st principal strain distribution of the corroded specimen (A7 as an example) at the final step of the 're-start' stage of analysis is shown in **Fig. 10**. It can be found that the concentration of the 1st principal strain denotes the possible position of the cracks in the specimen, including both the longitudinal and transverse cracks. Although the numerical results are still unable to give a precise esti-

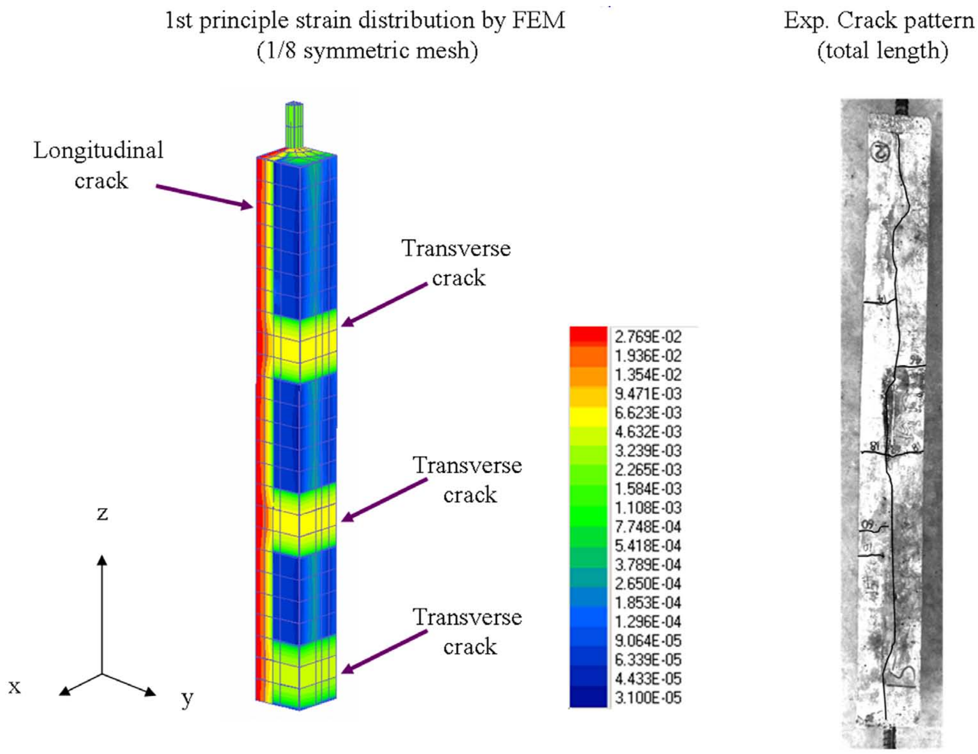

Fig. 10 Simulated 1st principal strain distribution at the surface of corroded specimen (A7) at final load.

mation of crack position (as compared with the experimentally obtained positions), the total transverse crack count (that is, the average transverse crack spacing) is simulated by the analysis; the total computed transverse crack count should be twice the value given in the figures, since a symmetric model is used for analysis. Here, the local bond deterioration around crack planes is bluntly taken into account as the 3D cone shaped crack propagation is numerically simulated.

Figure 11 shows a typical hoop tension strain distribution of the corroded specimens (specimen A7) at the same step as **Fig. 10**. Owing to the expansion of corrosive product, the hoop tension strain is localized in the longitudinal cracking surface in the view of the cross section. In addition, the hoop tension strain has a periodical distribution in the two longitudinal sections; the peak hoop strain always occurs at the loading end and transverse crack surface. Therefore, both the distribution of hoop strain can evidently prove the computed transverse crack number obtained from **Fig. 10**.

The computed load-deformation relation for the concrete and the computed longitudinal strain distribution for each specimen are compared with the experimental data in **Fig. 12 (a)-(i)**. To make it clear, only computed longitudinal strain distribution is shown here. Both the total transverse crack count (that is, the average transverse crack spacing) and the load-deformation relation are simulated well by the analysis. This is especially true for medium degrees of corrosion.

Lots of cracks are observed in the experiment and also computationally simulated in cases with a significant shrinkage effect (specimens A3, A4, and A6), but it seems that the numbers of cracks are not exactly coincident. This implies that the coupling effect of corrosion and shrinkage on bonding needs to be further investigated. These cases with significant shrinkage are excluded from **Fig. 13**, which summarizes this comparison of analytical and experimental results.

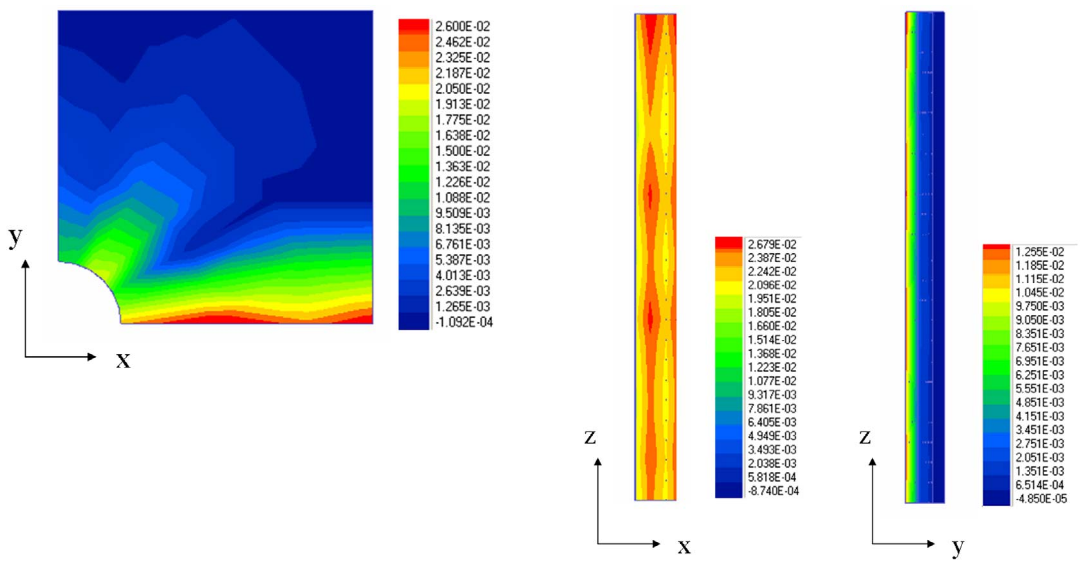

(a) In the view of cross section (b) In the view of longitudinal section

Fig. 11 Simulated hoop strain distribution of corroded specimen (A7) at final load.

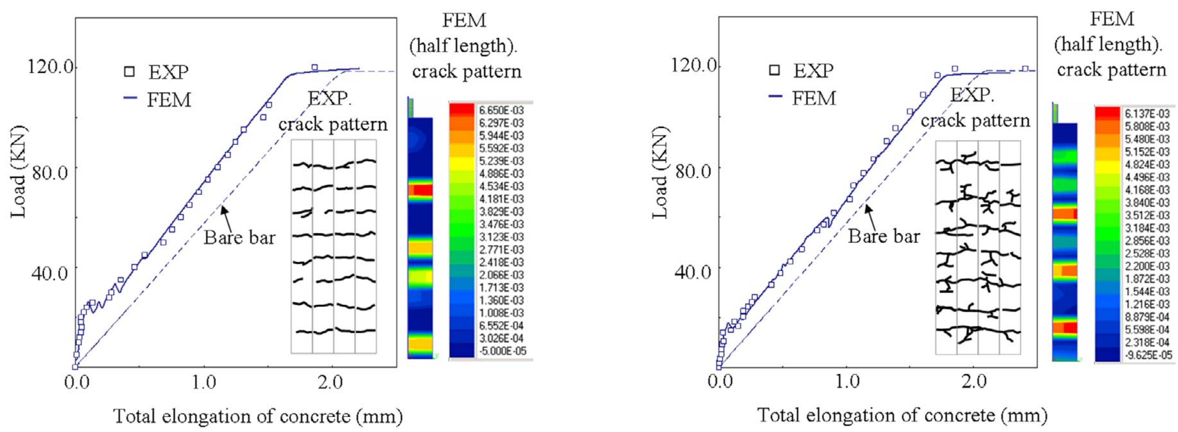

(a) Specimen A1/A2 (Transverse crack count Exp: 8, FEM: 8) (b) Specimen A3 (Transverse crack count Exp: 9, FEM: 12)

Fig. 12 Simulated load-elongation curve and crack pattern of each specimen.

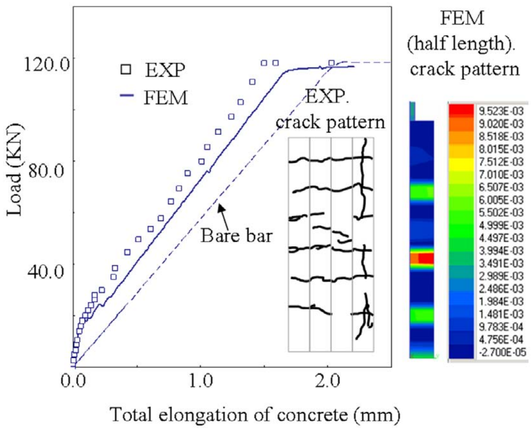

(c) Specimen A4 (Transverse crack count Exp: 7, FEM: 7)

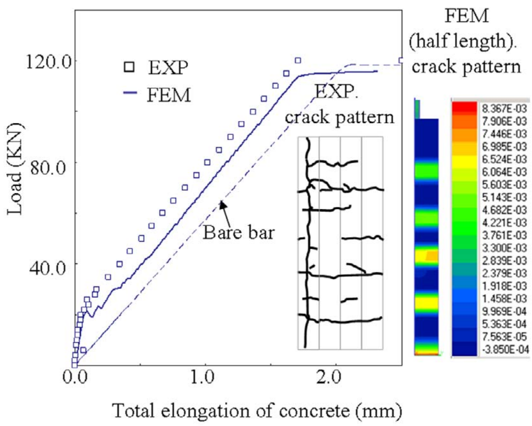

(d) Specimen A5 (Transverse crack count Exp: 7, FEM: 9)

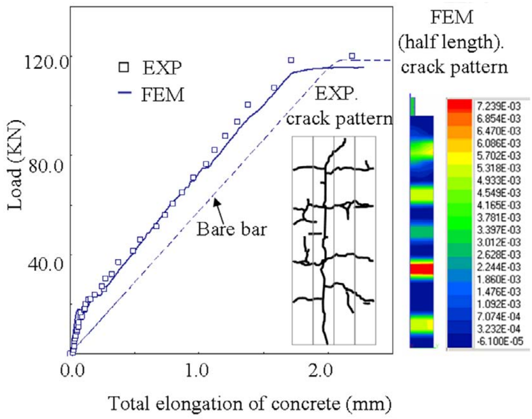

(e) Specimen A6 (Transverse crack count Exp: 7, FEM: 10)

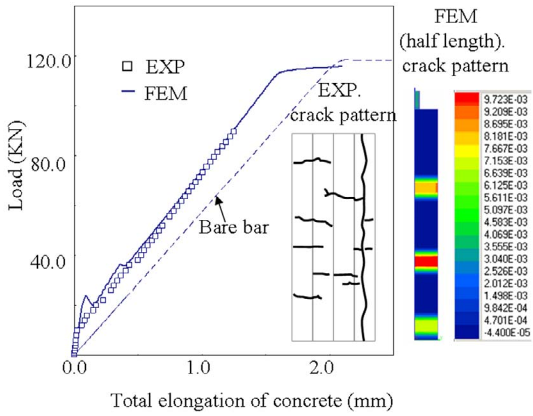

(f) Specimen A7 (Transverse crack count Exp: 6, FEM: 6)

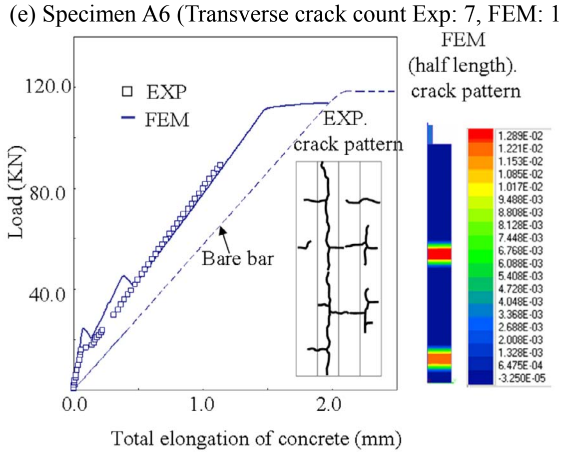

(g) Specimen A8 (Transverse crack count Exp: 4, FEM: 4)

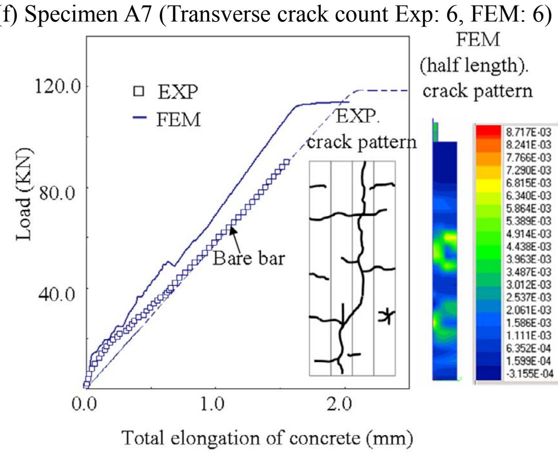

(h) Specimen A9 (Transverse crack count Exp: 5, FEM: 4)

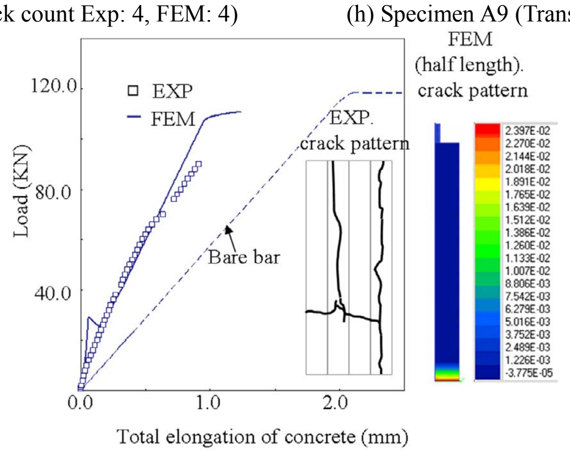

(i) Specimen A10 (Transverse crack count Exp: 1, FEM: 1)

Fig. 12 Simulated load-elongation curve and crack pattern of each specimen.

Table 4 Input parameters for simulation of the experiment by Amleh *et al*. (2006).

Specimen	Steel solid	Concrete solid	Interface element		
	ε_{expan}	f_t (MPa)	E_b^0(MPa/mm)	f_y (MPa)	η (μm)
SS1/SS2	0.0	1.7	1200.00	48.00	0.0
CS1	0.0065	1.7	1200.00	48.00	267.0
CS2	0.0080	1.7	1200.00	48.00	359.0
CS3	0.220	1.7	1200.00	48.00	2766.0
CS4	0.080	1.7	1200.00	48.00	1393.0
CS5	0.110	1.7	1200.00	48.00	1719.0
CS6	0.300	1.7	1200.00	48.00	3917.0

Further analysis is carried out to simulate the experiments carried out by Amleh *et al*. (2006). **Table 4** shows the input parameters in these cases. **Figure 14** gives the simulated transverse crack spacing versus corrosion level results compared with the experimental results; good agreement is achieved in this case also, which demonstrates the applicability of the extended open-slip coupled model and the corrosion pre-damage analytical approach.

5.4 Mechanical properties of corrosion products layer

Sensitivity analysis with different values of G_{cor} (1GPa, 0.01GPa) are carried out to check the assumption made in section 4. Analysis results for ultimate transverse crack count for these cases are also shown on the graph in **Fig. 13**. These results show that the modulus of the corroded layer also has an important influence on the total number of transverse cracks that arise from the analysis. Further, they prove the applicability of the original G_{cor} assumption and confirm the observations made by Ouglova *et al*. (2006).

Considering the bar-corrosion-concrete interactions, the layer of corrosion products serves as a bridge between the virgin steel and the surrounding concrete. The mechanical properties of this layer dominate stress transfer between the reinforcing bar and the concrete. Consequently, choosing too large or too small a value of G_{cor} will lead to incorrect evaluation of the post-corrosion residual bond behavior and thus to unrealistic predictions of the transverse crack count. Since the stiffness of the corrosion products is associated with the level of confinement at the interface, as already discussed, this parameter has to be considered when simulating the bond behavior after corrosion (section 5.3).

One point of note is that no transverse cracking occurs beyond a certain level of corrosion when G_{cor}=0.01GPa. This hints that it might be proper to use this value of G_{cor} when free expansion of the corrosion products is possible, as discussed above.

6. Conclusions

The tension-stiffening behavior of corroded reinforced concrete in tension was experimentally investigated. The open-slip coupled model of the concrete-steel bond transition zone was extended to include the more general case in which the reinforcement has corroded and a layer of corrosion products is present at the interface between steel and concrete. The following conclusions are reached as a result of this work:

(1) The experiments clarify that the residual bond performance after corrosion of the steel reinforcement is closely associated with the amount of transverse cracking (that is, associated with the average crack spacing in the corroded RC members).
(2) A simplified approach to three-dimensional nonlinear simulation of the bond transition zone, including

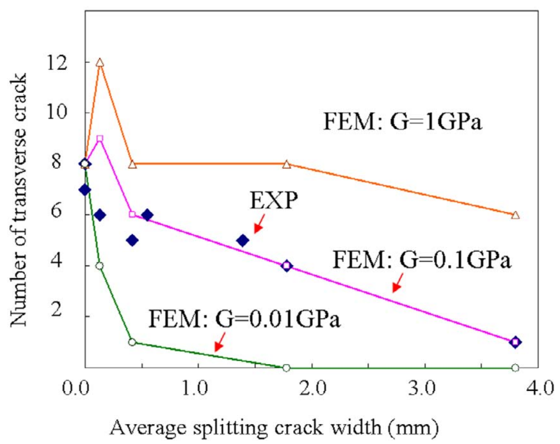

Fig. 13 Simulation of experiments by the authors.

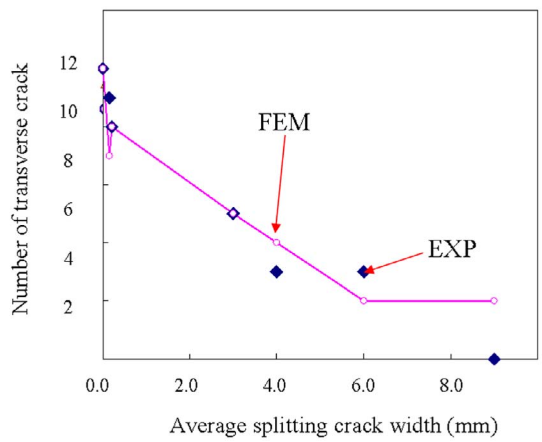

Fig. 14 Simulation of experiments by Amleh, *et al*. (2006).

the layer of corrosion products around the reinforcing bar, is developed. This finite element simulation correctly reproduces the crack spacing and space-averaged stiffness in tension. The open-slip coupled model may successfully take into account the magnified ring tension stress field associated with longitudinal bond action and the so-called corrosion pressure around bars.

(3) The group of individual microscopic constitutive models was comprehensively verified in terms of the overall tension nonlinearity of RC, but each micro-modeling should be more directly examined in future. Sensitivity analysis demonstrates that modeling of the bond transition zone and of the layer of corrosion products are the primary factors requiring attention so as to achieve further improvements and a more versatile simulation.

Acknowledgement

The authors express the gratitude to Dr. S. He and Prof. H. Wang's group at Shandong University of Technology for their assistance in conducting the experiments. The fourth author is grateful for financial support by Grant-in-Aid for Scientific Research (20246073) from Japan Society for the Promotion of Science.

References

Al-Suluimaini, G. J., Kaleemullah, M. and Basumbul, I. A., (1990). "Influence of corrosion and cracking on bond behavior and strength of reinforced concrete members." *ACI Structural Journal*, 87(2), 230-231.

Amleh, L. and Mirza, S., (1999). "Corrosion influence on bond between steel and concrete." *ACI Structural Journal*, 96(3), 415-423.

Amleh, L. and Ghosh, A., (2006). "Modeling the effect of corrosion on bond strength at the steel-concrete interface with finite-element analysis." *Canadian Journal of Civil Engineering*, 33(6), 673-682.

Auyeung, Y. B., balaguru, P. and Chung, L., (2000). "Bond behavior of corroded reinforcement bars." *ACI Material Journal*, 97(2), 214-220.

Berra, M., Castellani, A., Coronelli, D. Zanni, S. and Zhang, G., (2003). "Steel-concrete bond deterioration due to corrosion: finite-element analysis for different confinement levels." *Magazine of Concrete Research*, 55(3), 237-247.

Chou, L., Niwa, J. and Okamura, H., (1983). "Bond model for deformed bars embedded in massive concrete." *Proc. of 2nd JCI Colloquium on Shear Analysis of RC Structures, JCI.* 42-52.

Coronelli, D., (2002). "Corrosion cracking and bond strength modeling for corroded bars in reinforced concrete." *ACI Structure Journal,* 99(3), 267-276.

Coronelli, D. and Gambarova, P., (2004). "Structural assessment of corroded reinforced concrete beams: Modeling Guidelines." *Journal of Structural Engineering*, 130(8), 1214-1224.

Enright, M. P. and Frangopol, D. M., (1998). "Service prediction of deteriorating concrete bridges." *Journal of Structural Engineering,* 124(3), 309-317.

Fang, C., Lundgren, K., Chen, L. and Zhu, C., (2004). "Corrosion influence on bond in reinforced concrete". *Cement and Concrete Research*, 34(11), 2159-2167.

Fardis, M. N., (2009). "Seismic design, assessment and retrofitting of concrete buildings: Based on EN-Eurocode 8." *Geotechnical, Geological and Earthquake Engineering*, 8, *ISSN 1573-6059,* Springer Science and Business.

Hawkins, N. M., Lin I. J. and Jeang, F. L., (1982). "Local bond strength of concrete for cyclic reversed loading." *Bond in concrete,* Applied Science Publishers, London, 151–161.

Červenka, V., (2002). "Computer simulation of failure of concrete structures for practice." *1st fib Congress 2002 Concrete Structures in 21 Century*, Osaka, Japan, Keynote lecture, 289-304.

Li, C. Q., (2003). "Life-cycle modeling of corrosion-affected concrete structures: Propagation." *Journal of Structural Engineering*, 129(6), 753-761.

Lundgren, K., (2005). "Bond between ribbed bars and concrete. Part 2: The effect of corrosion." *Magazine of Concrete Research*, 57(7), 383-395.

Lundgren, K., (2007). "Effect of corrosion on the bond between steel and concrete: an overview." *Magazine of Concrete Research*, 59(6), 447-461.

Molina, F. J., Alonso, C. and Andrade, C., (1993). "Cover cracking as a function of rebar corrosion: Part 2-Numerical model." *Materials and Structures,* 26, 532-548.

Maekawa, K., Pimanmas, A. and Okamura, H., (2003). "*Nonlinear Mechanics of Reinforced Concrete*." *Spon Press*, London.

Ouglova, A., Berthaud, Y., Francois, M. and Foct, F., (2006). "Mechanical properties of an iron oxide formed by corrosion in reinforced concrete structures." *Corrosion Science*, 48, 3988–4000.

Rodriguez, J., Ortega, L. M. and Casal, J., (1997). "Load carrying capacity of concrete structures with corroded reinforcement." *Construction and Building Materials*, 11(4), 239-248.

Shang, F., An, X., Kawai, S. and Mishima, T., (2010). "Open-slip coupled model for simulating three-dimensional bond behavior of reinforcing bars in concrete." *Computers and Concrete*, 7(5), 403-419.

Shima, H., Chou, L. and Okamura, H., (1987). "Micro and macro models for bond in reinforced concrete." *J. Fac. Eng., Univ. Tokyo (B)*, 39(2), 133-194.

Tepfers, R., (1979). "Cracking of concrete cover along anchored deformed reinforcing bars." *Magazine of Concrete Research*, 31(106), 3-12.

Toongoenthong, K. and Maekawa, K., (2005). "Multi-mechanical approach to structural performance assessment of corroded RC members in Shear." *Journal of Advanced Concrete Technology*, 3(1), 107-122.

Xu, Y., Shen, W. and Wang, H., (1994). "An experimental study of bond-anchorage properties of bars in concrete." (in Chinese) *Journal of Building Structures*, 15(3), 27-36.

Yoshioka, Y. and Yonezawa, T., (1982). "Basic study about mechanical characteristics of reinforcement corrosion." *Proc. of the Annual Conference of the JSCE*, 271-272.

Zhang, R., Castel, A. and Francois, R., (2009). "The corrosion pattern of reinforcement and its influence on serviceability of reinforced concrete members in chloride environment." *Cement and Concrete Research*, 39(11), 1077-1086.